AIAA JOURNAL
Vol. 47, No. 5, May 2009

Arc Wind-Tunnel Flow Diagnostics by Cavity-Enhanced Absorption Spectroscopy

Hiroki Takayanagi*
Japan Aerospace Exploration Agency, Tokyo 182-8522, Japan
Makoto Matsui,† Kimiya Komurasaki,‡ and Hideaki Ochimizu§
University of Tokyo, Chiba 277-8583, Japan
and
Yoshihiro Arakawa¶
University of Tokyo, Tokyo 113-8656, Japan

DOI: 10.2514/1.39362

Cavity-enhanced absorption spectroscopy was applied to an arc wind-tunnel flow to measure the number density and the temperature distributions. With installed Brewster windows on a vacuum chamber, a cavity was constructed between a pair of high-reflectance mirrors placed outside of the chamber. Consequently, sensitivity was improved by more than 2 orders of magnitude compared with conventional single-pass laser absorption spectroscopy. The temperature distribution of 0.2% diluted oxygen estimated by cavity-enhanced absorption spectroscopy shows a good agreement with that of argon estimated by single-pass laser absorption spectroscopy.

Nomenclature

$A(\nu)$	=	absorbance, kd_0
A_{CEAS}	=	absorbance in CEAS $= kd_{\mathrm{CEAS}}$
A_{ij}	=	Einstein coefficient, s^{-1}
C_P	=	specific heat at constant pressure, $\mathrm{J/kg \cdot K}$
c	=	velocity of light, m/s
d	=	length of the optical cavity, m
d_{CEAS}	=	effective optical absorption path length in cavity-enhanced absorption spectroscopy, m
d_0	=	optical absorption path length, m
E_i	=	excitation energy at the absorbed state, eV
g	=	statistical weight
h_{chem}	=	chemical potential, MJ/kg
h_0	=	specific total enthalpy, MJ/kg
I_t	=	transmitted laser intensity, $\mathrm{mW/mm^2}$
I_0	=	incident laser intensity, $\mathrm{mW/mm^2}$
i, j	=	absorbing and excited state
K	=	integrated absorption coefficient, $\mathrm{GHz \cdot m^{-1}}$
k	=	absorption coefficient, m^{-1}
k_B	=	Boltzmann constant, J/K
M	=	Mach number
M_A	=	atomic mass, kg
m_e	=	electron mass, kg
N	=	number density, m^{-3}
R	=	gas constant, $\mathrm{J/kg \cdot K}$
R_{eff}	=	effective reflectance of the mirrors
T_{tr}	=	translational temperature, K
$T_{1,2}$	=	transmittance of the mirrors
u	=	flow velocity, m/s
z	=	sum of states
γ	=	specific heat ratio
$\Delta\nu_D$	=	full width at half-maximum of the Doppler profile, GHz
$\Delta\nu_L$	=	full width at half-maximum of the Lorentz profile, GHz
λ	=	laser wavelength, nm
ν	=	laser frequency, Hz
ν_0	=	center absorption frequency, Hz
χ_i	=	ionization energy, eV

I. Introduction

LASER absorption spectroscopy (LAS) has become a useful sensor strategy for fast, nonintrusive, and reliable in situ measurements of multiple flowfield parameters such as temperature, pressure, velocity, and species concentrations in widely varied fields [1–6].

In aerospace fields, LAS has been applied to rocket engine and shock-tunnel diagnostics. In our previous study, LAS was applied to flows generated in arc wind tunnels and in an inductive plasma generator for detecting absorption signals of the OI at 777.19 nm ($3s^5S \rightarrow 3p^5P$) line [7,8]. The results of these experiments revealed that the absorption signals were so small that they were detected only near the center axis in nitrogen/oxygen flow [9]. In another attempt of LAS undertaken in the NASA Ames Research Center interaction heating facility (60 MW) arc wind tunnel, Kim et al. [10] succeeded in the measurements of absorption of atomic oxygen and nitrogen in the arc heater region upstream of the nozzle throat, whereas they have not yet detected the absorption signal within its plume downstream of the nozzle expansion.

In this paper, cavity-enhanced absorption spectroscopy (CEAS), which is one of the cavity-based absorption methods [11–14], is applied to a plume of an arc wind tunnel. In this method, the laser signal intensity is maximized in the cavity-based methods because only the resonated signals are detected. That is why it is well fitted for high-enthalpy flow diagnostics with large emissions. To verify the applicability of CEAS to high-enthalpy flows, absorption profiles of 0.2% diluted oxygen were measured by CEAS and compared with those of argon measured by single-pass LAS.

Presented as Paper 3447 at the 39th AIAA Thermophysics Conference, Miami, FL, 25–28 June 2006; received 26 June 2008; revision received 8 December 2008; accepted for publication 26 December 2008.

*Researcher, Aerospace Research and Development Directorate, 7-44-1 Jindaiji Higashi-machi, Chofu-shi. Member AIAA.

†Japan Society for the Promotion of Science Research Fellow, Department of Aeronautics and Astronautics, 5-1-5 Kahiwanoha, Kashiwa-shi. Member AIAA.

‡Associate Professor, Department of Advanced Energy, 5-1-5 Kashiwanoha, Kashiwa-shi. Senior Member AIAA.

§Graduate Student, Department of Advanced Energy, 5-1-5 Kashiwanoha, Kashiwa-shi.

¶Professor, Department of Aeronautics and Astronautics, 7-3-1 Hongo, Bunkyo-ku. Senior Member AIAA.

II. Theory

A. Laser Absorption Spectroscopy

The decrease in laser beam intensity, dI, propagating in the x direction through an absorbing sample is expressed by the Beer–Lambert relation [15]:

$$\mathrm{d}I = -k_\nu I_0 \,\mathrm{d}x \tag{1}$$

where k_ν is a function of the laser frequency ν given by the following Voigt profile:

$$k_\nu = K\frac{2}{\Delta\nu_D}\sqrt{\frac{\ln 2}{\pi}}\int_{-\infty}^{\infty}\frac{\exp(-t^2)}{y^2+(x-t)^2}\,\mathrm{d}t$$
$$x = \frac{\sqrt{\ln 2}(\nu-\nu_0)}{\Delta\nu_D}, \qquad y = \frac{\sqrt{\ln 2}\Delta\nu_L}{\Delta\nu_D} \tag{2}$$

The number density of the absorption state i is related to the integrated absorption coefficient K:

$$K \equiv \int k_\nu \,\mathrm{d}\nu \approx \frac{\lambda^2}{8\pi}\frac{g_j}{g_i}A_{ji}N_i \tag{3}$$

The translational temperature is related to the Doppler width $\Delta\nu_D$:

$$T_{\mathrm{tr}} = \frac{c^2(\Delta\nu_D)^2 M_A}{(8\ln 2)k\nu_0^2} \tag{4}$$

B. Cavity-Enhanced Absorption Spectroscopy

For CEAS, a Fabry–Perot cavity consisting of two high-reflectance mirrors is used. Because the resonated laser beam can only transmit through the cavity, the target profiles should be larger than the free spectral range (FSR) of the cavity. In this study, the length of the optical cavity, d, was fixed to be 1.3 m (its FSR is about 115 MHz) in view of the absorption width of the target low-pressure plasma.

The transmitted laser intensity is calculated by the Fabry–Perot equation:

$$\frac{I_t}{I_0} = \frac{T_1 T_2 \exp(-kd_0)}{\{1-R_{\mathrm{eff}}\exp(-kd_0)\}^2} \tag{5}$$

where R_{eff} is the effective reflectance introduced to take into account energy losses in the laser beam through multiple reflection. From Eq. (5), the absorbance in single-pass LAS, kd_0, is related to that in CEAS, kd_{CEAS}, as

$$kd_{\mathrm{CEAS}} = -\ln\left(\frac{I_t}{I_0}\right)_{\mathrm{CEAS}} = -\ln\left[\frac{(1-R_{\mathrm{eff}})^2\exp(-kd_0)}{\{1-R_{\mathrm{eff}}\exp(-kd_0)\}^2}\right] \tag{6}$$

III. Experimental Setup

A. Measurement System

A schematic diagram of the measurement system for CEAS is illustrated in Fig. 1. A tunable diode laser with an external cavity (velocity model 6300, New Focus, Inc.) was used as the laser oscillator. It is not accompanied with mode hops in wide modulation width, achieving the stable measurements. The laser frequency was modulated over 20 GHz at approximately a 0.5 Hz repetition frequency by a function generator. High-reflectance concave mirrors with a 1-m-curvature radius (model 104750, Layertec, GmbH) were used for constructing a cavity. A lens with a 0.5 m focal length was used for mode matching [16]. A Faraday optical isolator was inserted between the tunable diode laser and the optics to reduce optical feedback to the laser diode. An etalon with a 0.75 GHz FSR was used to measure the frequency-modulation width. Emission from the plasma was shielded by a bandpass filter, the center wavelength and the full width at half-maximum of which are 780 and 10 nm, respectively. The transmitted laser intensity was measured by a photomultiplier tube (H8249-102, Hamamatsu Photonics KK). To apply A/D conversion and quick storage, a peripheral component interconnect digitizer (DP306, Agilent Technologies) with 12-bit resolution was used. This apparatus allows us to store 100 megasample data, which are necessary to diagnose one cross section, within 20 min.

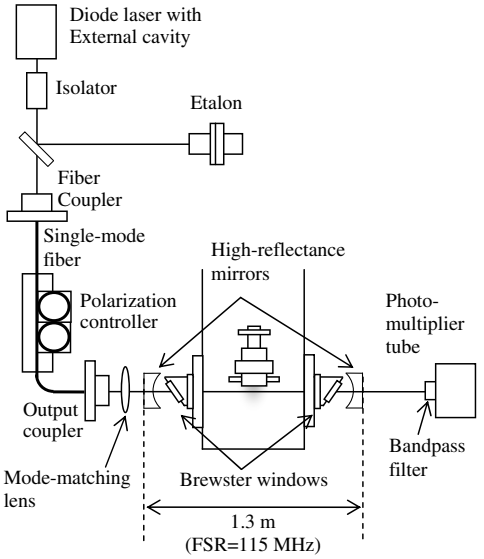

Fig. 1 A schematic diagram of the measurement system for cavity-enhanced absorption spectroscopy.

In this research, the absorption lines of ArI at 772.38 nm ($4s^2[3/2] \rightarrow 4p^2[3/2]$) and 772.42 nm ($4s^2[1/2] \rightarrow 4p^2[1/2]$) and OI at 777.19 nm ($3s^5S \rightarrow 3p^5P$) were used. The transition data of these lines are shown in Table 1 [17].

In CEAS, energy losses in the cavity due to optical windows degrade the signal-to-noise ratio. To minimize such effects, Brewster windows and a polarization controller (FPC030, Thorlabs, Inc.) were introduced. In Fig. 2, the ideal reflectance and transmittance of the laser beam at the quartz surface are plotted against the incident angle of the laser beam [18]. The incident laser at the Brewster angle transmits the window without energy losses.

B. Arc Wind Tunnel

A schematic of the arc wind tunnel is illustrated in Fig. 3. The cathode is made of 2% thoriated–tungsten alloy, and the nozzle as the anode is made of copper. Both electrodes are water-cooled. The constrictor is 2 mm in diameter and 3 mm in length. Argon mixed with oxygen by 0.2% in molar concentration was used as a working gas to simulate a low-number-density oxygen flow and was supplied through mass flow controllers. A 0.5-m-diam and 2-m-long cylindrical steel vacuum chamber made of steel is evacuated by a 1020 m^3/s mechanical pump backed by a 150 m^3/s rotary pump. The chamber pressure is maintained to be at 20 Pa with 0.149 g/s of argon and 2.38×10^{-4} g/s of oxygen flows. The arc wind tunnel was located on the center of the chamber, the plume of which was oriented parallel to the chamber axis. In addition, it was set on a translation stage to alter the height.

The operational condition is summarized in Table 2. Measurements were made at 50 mm downstream from the nozzle exit of the

Table 1 Transition data of atomic oxygen and argon

	O I	Ar I	Ar I
Lower state (1)	$3s^5S$	$4s^2[3/2]$	$4s^2[1/2]$
Upper state (2)	$3p^5P$	$4p^2[3/2]$	$4p^2[1/2]$
λ, nm	777.19	772.38	772.42
E_1, eV	9.15	11.55	11.72
E_2, eV	10.74	13.15	13.33
g_1	5	5	1
g_2	7	3	3
$A_{21}(10^7\ s^{-1})$	3.69	0.52	1.17

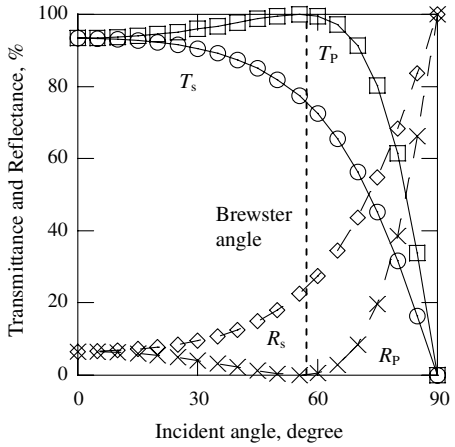

Fig. 2 Theoretical transmittance and reflectance of the *S* wave and *P* wave at the quartz surface.

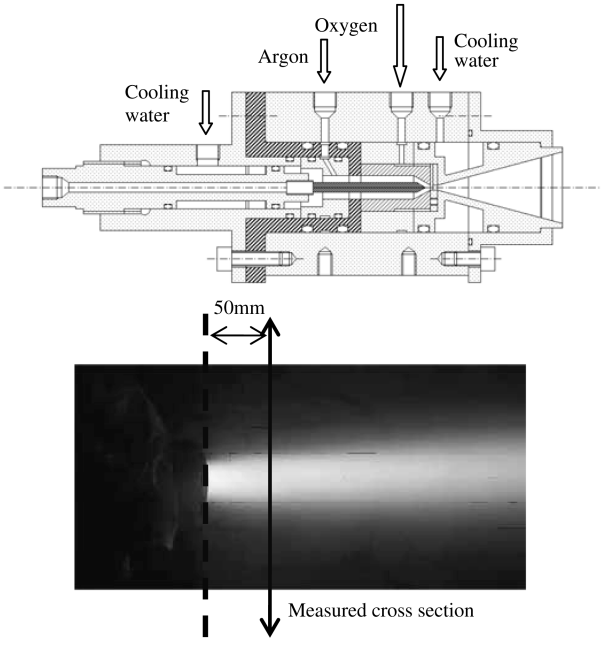

Fig. 3 Configuration of the arc wind tunnel (top) and a photo of the plume.

arc wind tunnel. Its input power, discharge current, and plenum pressure were 1.1 kW, 50 A, and 80 kPa, respectively.

IV. Results and Discussion

A. Estimation of Effective Reflectance

Equation (6) shows that kd_{CEAS} is related to kd_0 through the effective reflectance of the mirror, R_{eff}. To determine R_{eff}, CEAS signals of argon lines at 772.38 and 772.42 nm at 40, 45, 50, and 65 mm from the center axis were measured. Figure 4 shows kd_0 deduced by CEAS (circle) and single-pass LAS (solid line) at 45 mm. Fitted by Eq. (5), the reflectance of the mirror was estimated as

Table 2 Operational conditions of constricted arc wind tunnel

Operational condition	Value
Working gas (Mass flow rate)	Ar (0.149 g/s), O_2 (2.38×10^{-4} g/s)
Input power	1.1 kW
Input current	50 A
Mach number	2 (designed)
Plenum pressure	80 Pa
Chamber ambient pressure	20 Pa

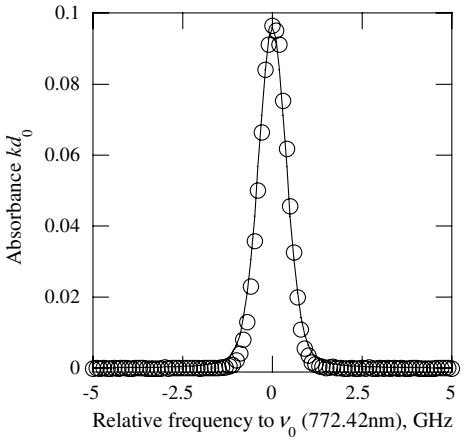

Fig. 4 Absorbance kd_0 deduced by CEAS (circle) and single-pass LAS (solid line) at 45 mm from the center axis of the arc wind-tunnel flow. Fitted by Eq. (5), the reflectance of the mirrors was estimated as 99.28%.

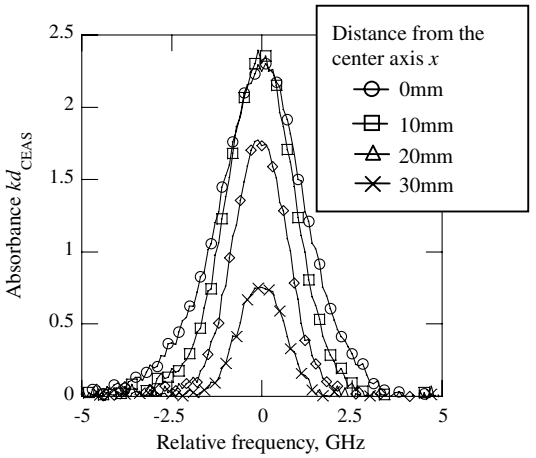

Fig. 5 Measured absorption profiles by cavity-enhanced absorption spectroscopy at each height from the center axis of the arcjet flow.

$$R_{\mathrm{eff}} = (99.3 \pm 0.05)\% \tag{7}$$

B. Number Density and Temperature Distributions

The number density and the temperature distribution in the arc wind-tunnel flow were deduced from an absorption line of OI at the center frequency of $\nu_0 = 777.19$ nm. The value of kd_{CEAS} was measured at every 2 mm distance from the center across the flow, as shown in Fig. 5. The value of kd_0 at each frequency was calculated by Eq. (6), as shown in Fig. 6. Because kd_0 was determined as a result of integration along the lines of sight, Abel inversion was applied to obtain the spatial distribution of the absorption coefficient [19]. Using the axisymmetric assumption for flow properties, the absorption coefficient is obtained by the Abel inversion:

$$k(\nu) = -\frac{1}{\pi}\int_r^R \frac{\mathrm{d}\{\ell_n[-(I_t/I_0)(x,\nu)]\}/\mathrm{d}x}{\sqrt{x^2 - r^2}}\mathrm{d}x \tag{8}$$

where r is the distance between the flow axis and the laser path. It was found that direct use of the measured data for I_t/I_0 results in an unsuccessful inversion, due to noises in the signal. To cope with this problem, the absorbance profile measured at each distance was first fitted by the following equation:

$$\ell_n[(I_t/I_0)(x,\nu)] = \left(\sum_{n=0}^{4} a_n x^{2n}\right)\exp(-\alpha x^2) \tag{9}$$

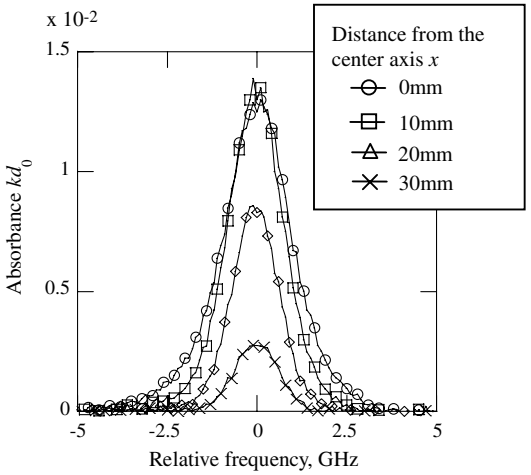

Fig. 6 Calculated absorption profiles by Eq. (6).

The absorbance was determined at every 0.1 GHz through interpolation. Finally, by applying the Abel inversion at each frequency, the absorption profile was successfully obtained at each radial position from the center.

Figure 7 shows the integrated absorption coefficients of argon and oxygen lines. It is seen that, using the CEAS system, the detectable limit can be decreased by more than 2 orders of magnitude, in comparison with the single-pass LAS system. Figure 8 shows the number density distributions of the argon atoms and oxygen atoms at the excited state, obtained by Eq. (3). The translational temperature is deduced by Eq. (4) from the full width at half-maximum of the Gaussian profile fitted to the measured absorbance profile. The radial distribution of the obtained temperature is shown in Fig. 9. It is seen that the temperatures deduced from the atomic lines of argon and oxygen show good agreement with each other, suggesting the accuracy of the CEAS measurement.

To assess the accuracy of the density and the temperature obtained by the CEAS measurement, the averaged temperature and the chemical composition in the flow are roughly estimated from the energy balance as follows. With an assumption of isentropic expansion, the total specific enthalpy is written as

$$h_0 = \int_0^{T_0} C_p \, \mathrm{d}T' + h_{\mathrm{chem}} = \int_0^{T} C_p \, \mathrm{d}T' + h_{\mathrm{chem}} + \frac{1}{2}u^2 \qquad (10)$$

The latter h_{chem} is constant under the chemically-frozen-flow assumption. The flow velocity u is expressed as

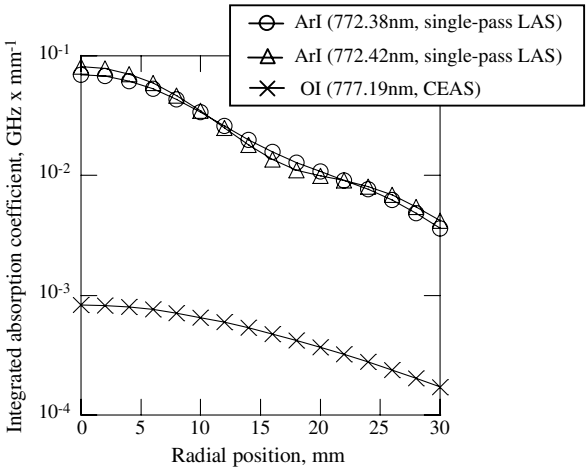

Fig. 7 Integrated absorption coefficients of absorbers in the arc wind-tunnel flow; the argon lines were measured by single-pass LAS and the oxygen line was measured by CEAS.

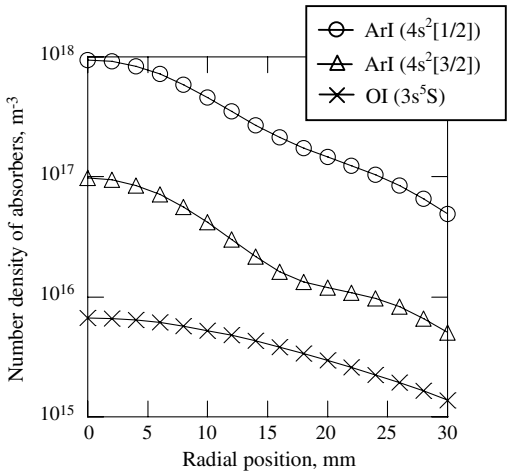

Fig. 8 Number density distribution for ArI ($4s^2$[1/2]), ArI ($4s^2$[3/2]) and OI ($3s^5$S) measured in the arc flow.

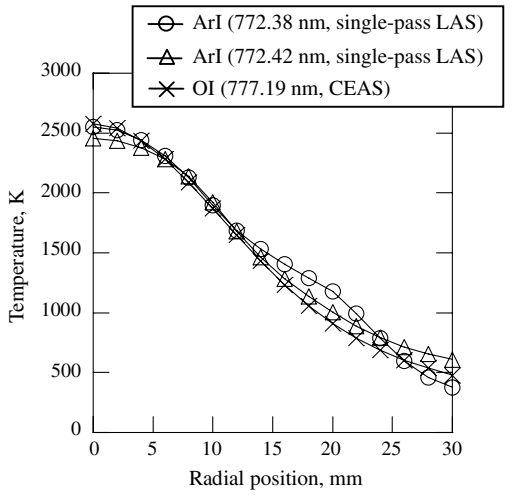

Fig. 9 Temperature distribution in the arc wind-tunnel flow.

$$u = M\sqrt{\gamma RT} \qquad (11)$$

The velocity was deduced from the design Mach number, 2, and the measured static temperature. The total pressure p_0 measured in the plenum chamber using a pressure sensor was as high as 80 kPa. Therefore, the chemical composition in the plenum chamber of the flow was calculated assuming thermochemical equilibrium. In that calculation, seven chemical species were considered (Ar, O_2, O, Ar+, O_2+, O+, and e−) in addition to four chemical reactions ($\mathrm{Ar} \leftrightarrow \mathrm{Ar}^+ + \mathrm{e}^-$, $\mathrm{O}_2 \leftrightarrow 2\mathrm{O}$, $\mathrm{O} \leftrightarrow \mathrm{O}^+ + \mathrm{e}^-$, and $2\mathrm{O} \leftrightarrow \mathrm{O}_2^+ + \mathrm{e}^-$). Their equilibrium constants were obtained from [20,21]. The averaged fraction of the O atom population in the $3s^5S$ state was calculated as 3.4×10^{-6}. The averaged fractions of the Ar atom population in the $4s^2[3/2]$ and $4s^2[1/2]$ states were calculated as 3.6×10^{-7} and 1.7×10^{-8}, respectively. The measured densities of excited oxygen and argon atoms were only a tiny fraction of all the oxygen and argon atoms, because the lower states of the absorption are approximately 9 and 11 eV above the ground states. The averaged h_0 within the radius of the nozzle exit, 15 mm, was estimated to be about 2.4 MJ/kg; the efficiency of the arc heater was about 30%, which can also be validated by the estimation by the temperature rise in the temperature of cooling water.

V. Conclusions

In this study, cavity-enhanced absorption spectroscopy was applied to the arc wind tunnel with oxygen diluted in argon as the

working gas. The results show that the sensitivity can be improved by more than 2 orders of magnitude by the CEAS method, in comparison with the conventional single-pass laser absorption spectroscopy. The temperature deduced by the CEAS method agreed well with that estimated by the single-pass LAS method. This suggests that the CEAS method has the potential of considerably improving the sensitivity without losing accuracy in temperature measurement.

Acknowledgments

The work was supported by Research Fellowships of the Japan Society for the Promotion of Science for Young Scientists, 19-3454, 2007, sponsored by the Ministry of Education, Culture, Sports, Science and Technology of Japan.

References

[1] Klaassen, J. J., Coy, S. L., and Steinfeld, J. I., "State-to-State Rotational Energy Transfer Measurements in Methane (CHD_3) by Infrared Double Resonance with a Tunable Diode Laser," *Journal of Chemical Physics*, Vol. 100, No. 8, 1994, pp. 5519–5532. doi:10.1063/1.467170

[2] Cooper, D. E., Martinelli, R. U., Carlisle, C. B., Riris, H., Bour, D. B., and Menna, R. J., "Measurement of $^{13}CO_2$:$^{12}CO_2$ Ratios for Medical Diagnostics with 1.6-μm Distributed-Feedback Semiconductor Lasers," *Applied Optics*, Vol. 32, No. 33, 1993, pp. 6727–6731.

[3] Iwasaki, M., Takeda, K., Masafumi, I., Yara, T., Uehara, T., and Hori, M., "Effect of Low Level O_2 Addition to N_2 on Surface Cleaning by Nonequiliburium Atmospheric-Pressure Pulsed Remote Plasma," *Japanese Journal of Applied Physics*, Vol. 46, No. 23, 2007, pp. L540–L542. doi:10.1143/JJAP.46.L540

[4] Puiu, A., Giubileo, G., and Bangrazi, C., "Laser Sensors for Trace Gases in Human Breath," *International Journal of Environmental and Analytical Chemistry*, Vol. 85, Nos. 12–13, 2005, pp. 1001–1012. doi:10.1080/03067310500154395

[5] Zhang, F. Y., Fujiwara, T., Komurasaki, K., Miyashita, T., and Harada, J., "Determination of Parameters in Arcjet Plume by Tomographic Reconstruction," *Transactions of the Japan Society for Aeronautical and Space Sciences*, Vol. 43, No. 140, 2000, pp. 77–87. doi:10.2322/tjsass.43.77

[6] Langlois, S., Birbeck, T. P., and Hanson, R. K., "Temperature-Dependent Collision-Broadening Parameters of H_2O Lines in the 1.4 μm Diode-Laser Absorption-Spectroscopy," *Journal of Molecular Spectroscopy*, Vol. 167, No. 2, 1994, pp. 272–281. doi:10.1006/jmsp.1994.1234

[7] Matsui, M., Takayanagi, H., Oda, Y., Komurasaki, K., and Arakawa, Y., "Performance of Arcjet-Type Atomic-Oxygen Generator by Laser Absorption Spectroscopy and CFD Analysis," *Vacuum*, Vol. 73, Nos. 3–4, 2004, pp. 341–346. doi:10.1016/j.vacuum.2003.12.046

[8] Matsui, M., Komurasaki, K., Herdrich, G., and Auweter-Kurtz, M., "Enthalpy Measurement in Inductively Heated Plasma Generator Flow by Laser Absorption Spectroscopy," *AIAA Journal*, Vol. 43, No. 9, 2005, pp. 2060–2064. doi:10.2514/1.14128

[9] Matsui, M., Komurasaki, K., Arakawa, Y., Knapp, A., Herdrich, G., and Auweter-Kurtz, M., "Enthalpy Measurement of Inductively Heated Airflow," *Journal of Spacecraft and Rockets*, Vol. 45, No. 1, 2008, pp. 155–157. doi:10.2514/1.34369

[10] Kim, S., Jeffries, J. B., and Hanson, R. K., "Measurement of Gas Temperature in the Arc-Heater of a Large Scale Arcjet Facility Using Tunable Diode Laser Absorption," AIAA Paper 2005-0900, Jan. 2005.

[11] Matsui, M., Yokota, S., Sako, D., Komurasaki, K., and Arakawa, Y., "Number Density Distributions of Xenon Atom in Hall Thruster Plumes," AIAA Paper 2007-5306, July 2007.

[12] Zybin, A., Kuritsyn, Y. A., Mironinko, V. R., and Niemax, K., "Cavity Enhanced Wavelength Modulation Spectrometry for Application in Chemical Analysis," *Applied Physics B (Lasers and Optics)*, Vol. 78, No. 1, 2004, pp. 103–109. doi:10.1007/s00340-003-1342-0

[13] Nakagawa, K., Katsuda, T., Shelkovnikov, A. S., Labachelerie, M., and Ohtsu, M., "Highly Sensitive Detection of Molecular Absorption Using a High Finesse Optical Cavity," *Optics Communications*, Vol. 107, Nos. 5–6, 1994, pp. 369–372. doi:10.1016/0030-4018(94)90349-2

[14] Berden, G., Peeters, R., and Meijer, G., "Cavity-Enhanced Absorption Spectroscopy of the 1.5 μm Band System of Jet-Cooled Ammonia," *Chemical Physics Letters*, Vol. 307, Nos. 3–4, 1999, pp. 131–138. doi:10.1016/S0009-2614(99)00504-7

[15] Davis, C. C., *Lasers and Electro-Optics*, Cambridge Univ. Press, Cambridge, England, U.K., 2005.

[16] Kogelnik, H., and Li, T., "Laser Beams and Resonators," *Applied Optics*, Vol. 5, No. 10, 1966, pp. 1550–1567. doi:10.1364/AO.5.001550

[17] *NIST Atomic Spectra Database* [online database], Ver. 3, http://physics.nist.gov/cgi-bin/AtData/main_asd [retrieved 26 Jan. 2009].

[18] Griem, H. R., *Principles of Plasma Spectroscopy*, Cambridge Univ. Press, Cambridge, England, U.K., 2005.

[19] Deutsch, M., "Abel Inversion with a Simple Analytic Representation for Experimental Data," *Applied Physics Letters*, Vol. 42, No. 3, 1983, pp. 237–239. doi:10.1063/1.93892

[20] Gupta, R. N., Yos, J. M., Thompson, R. A., and Lee, K. P., "A Review of Reaction Rates and Thermodynamic and Transport Properties for an 11-Species Air Model for Chemical and Thermal Nonequilibrium Calculations to 30,000 K," NASA RP-1232, 1990.

[21] Matsuzaki, R., "Quasi-One-Dimensional Aerodynamics with Chemical Vibration and Thermal Nonequilibrium," *Transactions of the Japan Society for Aeronautical and Space Sciences*, Vol. 30, No. 90, 1988, pp. 243–258.

R. Lucht
Associate Editor